The Role of MR Imaging in Determination of Hepatocellular Carcinoma Response to Radioembolization Therapy

Essay

Submitted For Partial Fulfillment of Master Degree in Radiodiagnosis

Presented by

Rana Mamdouh Naeim Tolba
(M.B.B.CH**)**

Supervised By

Prof. Dr Mounir Sobhy Guirguis

Professor of Radiodiagnosis
Faculty of Medicine - Ain Shams University

Dr. Amr Mohammed Ismaeel Saadawy

Lecturer of Radiodiagnosis
Faculty of Medicine - Ain Shams University

Faculty of Medicin
Ain Shams Univeristy
2016

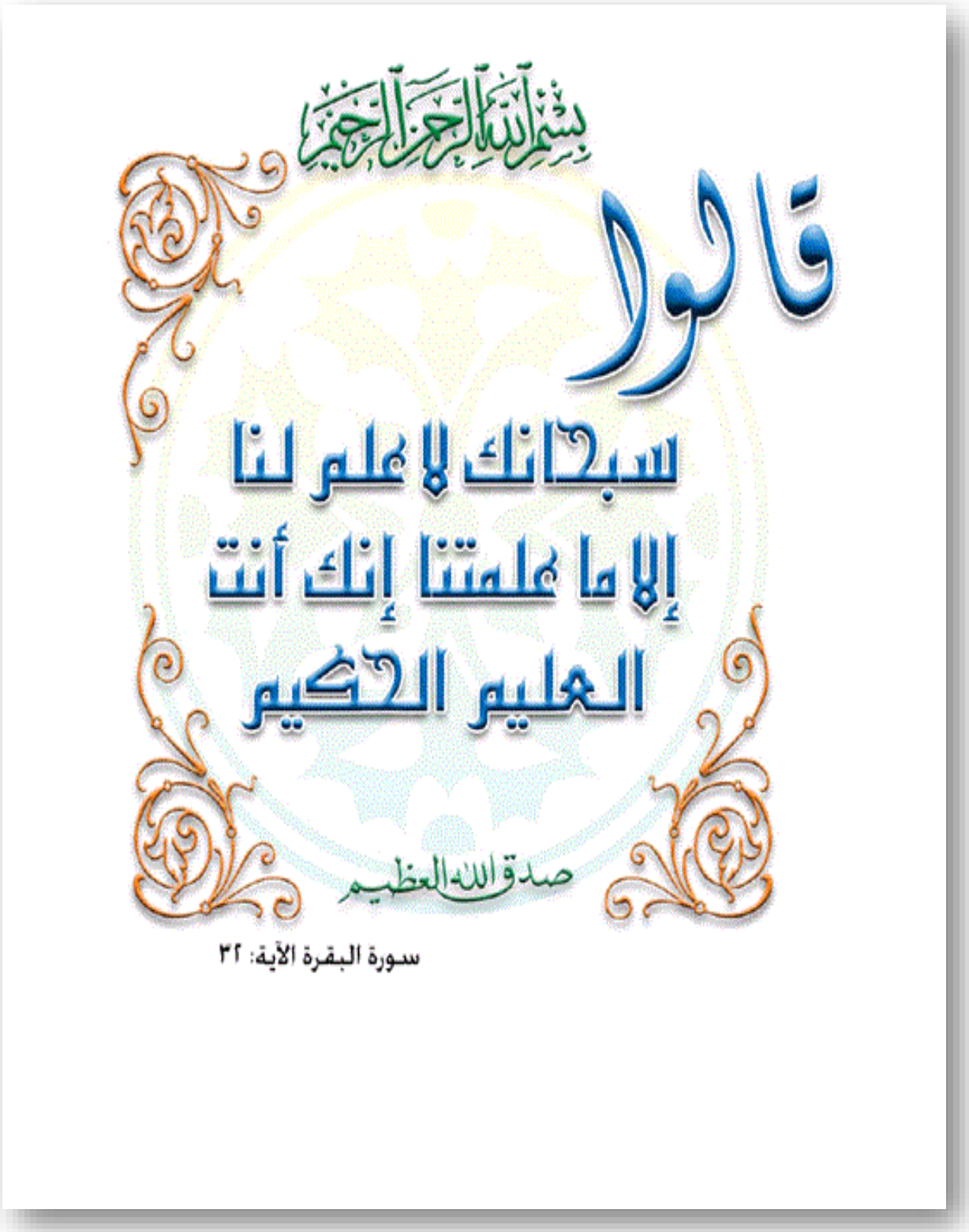
بسم الله الرحمن الرحيم
قالوا
سبحانك لا علم لنا
إلا ما علمتنا إنك أنت
العليم الحكيم
صدق الله العظيم
سورة البقرة الآية: ٣٢

Acknowledgement

First and foremost, my deep gratefulness and indebtedness is to Allah, the Most Gracious and the Most Merciful.

I would like to express my deepest appreciation and respect to Prof, Dr. Mounir Sobhy Guirguis, Professor of Radiodiagnosis, Faculty of Medicine- Ain Shams University, for his priceless effort, generous guidance and patience.

I am grateful to Dr. Amr Mohammed Ismaeel Saadawy, Lecture of Radiodiagnosis, Faculty of Medicine- Ain Shams University, for his great effort and patiency.

Lastly and not least, I send my deepest love to my family for their love and care.

Rana Mamdouh

LIST OF THE CONTENTS

Title	**Page No.**

- *List of Abbreviations………………………………......i*
- *List of figures…………………………………….......iv*
- *List of tables……………………………………….....x*
- *Introduction and aim of the work* **……..…………………....***1*
- *Chapter 1* **:**

  -MRI anatomy of the liver………………………………..*4*
- *Chapter 2* **:**

  -Pathology of hepatocellular carcinoma…………………*15*
- *Chapter 3 :*

  -Technical consideration ………………………………..*32*
- *Chapter 4* **:**

  -MRI finding in Hepatocellular carcinoma after Radioembolization therapy………………………………*59*
- *Summary and conclusion…………………...………80*
- *References……………………………………….…....83*
- *Arabic Summary*

LIST OF ABBREVIATIONS

3D	Three-dimension
3D GRE	Three-dimensional gradient-echo
ADC	Apparent diffusion coefficient
BCLC	Barcelona clinic liver cancer
BSA	Body surface area
CEA	Carcinoembryonic antigen
CEUS	Contrast Enhanced Ultrasound
CLD	Chronic liver disease
CT	Computed tomography
CTA	Computed tomography angiography
DWI	Diffusion weighted magnetic resonance imaging
EASL	European Association for the Study of the Liver
FDG	Fluorodeoxyglucose
FDG-PET/CT	Fluorine-18-2-fluoro-2-deoxy-D-glucose positron emission tomography
FSE	Fast spin-echo
GBCA	gadolinium-based contrast agent
GFR	Glumerular filtration rate
GRE	Gradient-recalled echo
HBV	Hepatitis B virus
HCC	Hepatocellular carcinoma

HCV	Hepatitis C viruses
ICCs	Intrahepatic cholangio carcinomas
IMV	Inferior mesenteric vein
IVC	Inferior vena cava
LPV	Left branch of the portal vein
m RECIST	Modified RECIST criteria
MAA	Macro-aggregated albumin
MDCT	Multi-detector computed tomography
MRI	Magnetic resonance imaging
N/C	Nuclear-to-cytoplasmic ratio
NSF	Nephrogenic systemic fibrosis
OS	Overall survival
PACT	Pelvi-abdominal computed tomography
PEI	Percutaneous ethanol injection
PET	Positron emission tomography
PFS	Progression free survival
PS	Performance status
RAS	Right anterior segment
RECIST	Response Evaluation Criteria in Solid Tumors
RFA	Radiofrequency ablation
RHA	Right hepatic artery

RILD	Radiation-induced liver disease
RPS	Right posterior segment
RPV	Right branch of the portal vein
SMV	Superior mesenteric vein
SPAIR	Spectral adiabatic inversion recovery
SPIO	Super paramagnetic iron oxide
SV	Splenic vein
TACE	Trans arterial chemoembolization
TARE	Trans arterial Radioembolization
WHO	World Health Organization

LIST OF FIGURES

Figures No.	Title	Page No.
Figure 1.1	Gross anatomical lobes of the liver	4
Figure 1.2	Axial T1-weighted MR image shows normal anatomy of the liver	5
Figure 1.3	Couinaud Scheme: the liver is divided into eight segments determined according to the main branches of the portal vein and the hepatic veins	6
Figure 1.4	Segments of the liver .	7
Figure 1.5	axial T2W MR images of the liver show the segmental anatomy of the liver.	8&9
Figure 1.6	Axial T1-weighted post contrast image of the liver shows the origin of celiac trunk.	9
Figure 1. 7	The hepatic artery branches	10
Figure 1.8	Hepatic angiogram shows the arterial anatomy of the liver.	10
Figure 1. 9	PACT with contrast shows Characteristic run of the left hepatic artery within the groove of Arantius, originating from the left gastric artery .	12
Figure 1.10	Gradient echo [GRE] portovenous-phase image clearly demonstrates normal portal-venous anatomy	12
Figure 1.11	Normal anatomy of the portal-venous system.	13
Figure 1.12	T1WI MRI post contrast study during portal venous phases through cephalic part of the liver	14

Figure 2.1	Gross pathology photograph of resected specimen	16
Figure 2.2	Photomicrograph shows trabecular pattern of HCC with intracytoplasmic fat and Mallory hyaline	17
Figure 2.3	Histology of a well-differentiated HCC. Hematoxylin and eosin staining	17
Figure 2.4	Histology of a moderately differentiated HCC. Hematoxylin and eosin staining	18
Figure 2.5	Fibrolamellar hepatocellular carcinoma (HCC)	19
Figure 2.6	MDCT and EOB-enhanced arterial phase MR image demonstrate a hypervascular nodule in patient with a history of hepatitis C cirrhosis (Child-Pugh A) and biopsy-proven moderately differentiated HCC	24
Figure. 2.7	Abdominal ultrasound of the liver	25
Figure. 2.8	Doppler abdominal ultrasound	26
Figure 2.9	Multi-detector computed tomography of hepatocellular carcinoma.	27
Figure 2.10	Multiphasic CT Images in a 51-year-old man with HCC and hepatitis B–related cirrhosis	28
Figure 2.11	MR technique with extracellular contrast agent in 64-year-old man with HCC and hepatitis B–related cirrhosis	29
Figure 2.12	MR imaging of 63-year-old man with HCC showing restricted diffusion	30
Figure 2.13	Hepatic angiography	31
Figure 3.1	MRI of liver cirrhosis with HCC showing typical HCC with hypointensity at T1WI, hyperintensity at T2WI.	38
Figure 3. 2	MRI of HCC in a 54-year-old woman with chronic hepatitis C. HCC appears mildly hyperintense to liver on the T2WI& hypo- to	38

	isointense on the T1WI.	
Figure 3.3	**MRI of 50 years old patient with HCC. T1-weighted in-phase & opposed phase image shows the tumor in segment II of the liver shows lower signal in the tumor indicating steatosis.**	**39**
Figure 3.4	**MR in 61-year-old man with hepatitis C–related cirrhosis, ligament is minimally hyperintense to adjacent parenchyma on T1-weighted in-phase image and hyperintense on T2-weighted fast-recovery fast spin-echo**	**39**
Figure 3.5	**MR images in a 46-year-old man with hepatitis B–related cirrhosis and HCC show restricted diffusion**	**41**
Figure 3.6	**Multiphasic MR Images with extracellular contrast agent in 64-year-old man with HCC and hepatitis B–related cirrhosis show large hypointense mass on precontrast image with hyperenhancement in late hepatic arterial phase**	**42**
Figure 3.7	**MR images in a 66-year-old man with HCC show corona enhancement and capsule appearance.**	**44**
Figure 3.8	**Multiphasic MR images with gadoxetate disodium in 42-year-old man with HCC and hepatitis B–related cirrhosis show large hypointense mass on precontrast image & hyperenhancement in late hepatic arterial phase& show apparent washout of contrast material from tumor in porto-venous phase**	**45**
Figure 3.9	**T1-weighted 3D GRE MR images with fat suppression show HCC in left lobe. Peripheral enhancing rim consistent with capsule appearance**	**47**
Figure 3.10	**T1-weighted three-dimensional (3D) gradient-echo (GRE) MR image with fat suppression obtained in late hepatic arterial phase after administration of gadolinium-**	**47**

	based contrast agent shows hyper enhancing mass with mosaic architecture in segment VII	
Figure 3.11	Gadoxetate disodium–enhanced T1-weighted 3D GRE MR image shows nodule hypointense on hepatobiliary phase image acquired 20 minutes after injection.	49
Figure 3.12	T2-weighted image after SPIO administration shows a large mass in the left lobe and multiple smaller lesions in the right lobe	51
Figure 3.13	Celiac angiogram obtained at initial radioembolization shows hypervascular tumor staining	56
Figure 3.14	left hepatic artery angiography demonstrates the accessory left gastric artery	56
Figure 3.15	Aortogram demonstrates replaced common hepatic artery& right hepatic artery	57
Figure 4.1	Contrast-enhanced MR 12 month after radioembolization demonstrates complete necrosis of the entire tumor with marked reduction in size.	61
Figure 4.2	T1- weighted gadolinium-enhanced MRI in the coronal plane demonstrates a large right lobe HCC with satellite lesions. demonstrates marked size reduction with near complete resolution of the tumor mass22 months after treatment with Y90	61
Figure 4.3	gadolinium-enhanced T1-weighted imaging demonstrates complete necrosis and avascularity of the caudate lobe HCC	63
Figure 4.4	MR image demonstrates HCC in the right hepatic lobe & Posttreatment MR image shows a slight decrease in tumor size but significant necrosis	63
Figure 4.5	Gadolinium-enhanced fat-suppressed T1-weighted MR image shows a well-defined tumor in the left hepatic lobe. 6 months after 90Y treatment shows complete response	64

Figure 4.6	**DWMRI shows a response with the mass showing less restricted diffusion and appearing significantly smaller. A new lesion is seen in the right lobe of the liver**	**66**
Figure 4.7	**Diffusion-weighted MR image obtained following ^{90}Y therapy shows increased water mobility (decreased signal intensity) in the treated area a finding that represents response**	**67**
Figure 4.8	**Gadolinium-enhanced T1-weighted imaging demonstrates complete necrosis and avascularity of the caudate lobe HCC. There is very little tumor shrinkage and thus no change in categorization .Serum AFP values continued to decline to 3 ng/dL, representing a 99.9% reduction**	**68**
Figure 4.9	**T1- weighted gadolinium-enhanced MRI demonstrates tumor necrosis and surrounding hepatic parenchymal hyperenhancement from radiation occurring in a perivascular distribution**	**69**
Figure 4.10	**MRI shows innumerable slightly hypointensr lesions on T1WI within the liver , which demonstrate ring enhancement reflecting treated HCC**	**70**
Figure 4.11	**Contrast-enhanced T1-weighted imaging at 2- year follow-up demonstrates heterogeneous enhancement of the hepatic parenchyma with capsular retraction, consistent with hepatic fibrosis in the Y90-treated right hepatic artery distribution**	**71**
Figure 4.12	**MRI obtaiened six months after Y90 radioembolization for HCC shows no hypervascularity within the tumor with capsular retraction and fibrotic enhancement within the mass anteriorly indicating intramural radiation fibrosis**	**72**
Figure 4.13	**6 months after TARE, follow-up contrast-enhanced MRI showed right lobe radiation effect with hyper enhancement and contra**	**73**

	lateral left liver lobe hypertrophy	
Figure 4.14	**MRI one year after Y90 embolization treatment of multifocal HCC to the right hepatic lobe shows the atrophic changes of segment 6 and 7 with arterial enhancement that persist in the portovenous phase ,representing radio fibrosis &demonstrates significant left lobe hypertrophy**	**73**
Figure 4 .15	**On 6-month follow-up, contrast-enhanced MRI shows the lack of enhancement from tumor necrosis with peripheral rim enhancement and hyperenhancement in the posterior sector from hyperemia from radiation effect**	**74**
Figure 4.16	**MRI obtained following treatment with 90Y demonstrates perihepatic fluid & Pleural effusion.**	**75**
Figure 4.17	**Pretreatment MR image shows tumoral mass with low signal intensity in the lateral aspect of the right lobe of the liver. After treatment with Y90 radioembolization, there is near-complete resolution of the mass. However, biliary dilation secondary to focal stricture is identified**	**76**
Figure 4.18	**Gadolinium -enhanced MRI of a patient with HCC treated with Y90. The patient developed a gastroduodenal ulcer following therapy**	**79**

LIST OF TABLES

Table No.	Title	Page No.
Table 3.1	Main characteristics and differences between Thera-Sphere and Sir-Spheres	53
Table 4.1	Criteria for Assessment of Response to ^{90}Y Microsphere Treatment Assessed with CT and MRI	60

Abstract

Hepatocellular carcinoma (HCC) is an aggressive primary liver malignancy, represents over 90% of all primary liver malignancy. Imaging plays a critical role in the diagnosis, staging, surveillance, and treatment monitoring of hepatocellular carcinoma (HCC). Unlike most malignancies, which typically require biopsy for diagnosis, HCC can be diagnosed based on MRI characteristics alone due to the relatively high specificity of this modality

HCC most commonly presents late in the disease course. As a result, the majority of patients are not candidates for curative therapies. Loco regional therapies including Yttrium-90 (Y-90) Radioembolization play an important role in management of the vast majority of patients with HCC.

KEYWORDS: Hepatocel.lular carcinoma, Dosimetry; Radioembolization of liver malignancies; Yttrium-90 microspheres

Introduction

Hepatocellular carcinoma (HCC) is the sixth most common cancer worldwide and the third most common cause of cancer mortality, it is diagnosed in more than half a million people per year worldwide.**(El-Serag, 2011).**

Despite the scientific advances and the implementation of measures for the early detection of HCC in patients at risk, the survival has not improved. This is due to the advanced stage of the disease at the time of clinical presentation and limited therapeutic options.

The therapeutic options fall into five main categories: surgical interventions including tumor resection and liver transplantation, percutaneous interventions including ethanol injection and radiofrequency thermal ablation, transarterial interventions including